Eur. Phys. J. B **40**, 93–102 (2004)
DOI: 10.1140/epjb/e2004-00243-5

THE EUROPEAN PHYSICAL JOURNAL B

Mesoscopic transport through toroidal carbon nanotubes threaded with a THz magnetic flux

H.-K. Zhao[1,2,a] and J. Wang[2]

[1] Department of Physics, Beijing Institute of Technology, Beijing 100081, P.R. China
[2] Department of Physics, The University of Hong Kong, Pokfulam Road, Hong Kong, P.R. China

Received 22 February 2004 / Received in final form 31 May 2004
Published online 3 August 2004 –

Abstract. We have investigated the quantum transport through mesoscopic systems with a toroidal carbon nanotube coupled with two metal leads (N-TCN-N) threaded with an ac magnetic flux. The energy shifting takes place by applying the magnetic flux, and this shifting arises from both the dc and ac components of magnetic flux. The dc magnetic flux ϕ induces the periodic variation of energy gap E_g of the TCN, and the ac magnetic flux component always increases the energy gap. As the photon energy is larger than the energy gap $\hbar\omega > E_g$, the electrons in the valence band can jump to the conductance band at zero temperature, and the tunneling current appears for $eV > E_g/2 + n\hbar\omega$, $(n = 0, \pm 1, \pm 2...)$. The differential conductance and tunneling current display clear effect of ac flux by modifying the current oscillation structures. The photon-assisted tunneling current exhibits stair-like I-V characteristics, and it shows different behaviors for different TCN systems. The magnitude of the current is suppressed by the applied ac flux. We also present the time-dependent current evolution, which is contributed by the oscillating current components.

PACS. 73.40.-c Electronic transport in interface structures – 73.63.Fg Nanotubes – 73.61.Wp Fullerenes and related materials – 73.22.-f Electronic structure of nanoscale materials: clusters, nanoparticles, nanotubes, and nanocrystals

1 Introduction

Recently, the single-wall carbon nanotubes (SWCNs) has attracted much attention due to their prospective applications on the electronic nano-devices. One of the important properties is the metal-semiconductor transition for different structures of SWCN. Because of the specific structure and electronic properties, we can employ these materials to study one-dimensional transport, such as those extensively investigated semiconductor quantum wire and hybrid device systems [1–8]. The resonant tunneling behavior in the SWCN based magnetic tunneling junctions as well as the dynamic conductance in the SWCN system due to an ac field are also studied [9]. As the two ends of a SWCN connect to form a closed toroidal carbon nanotube (TCN), the detailed carbon nanotube (CN) structure takes the central role for the conducting behavior, since the TCN is quantized in both of the longitudinal and transverse directions. The tori proposed are constructed by introducing a single pentagon-heptagon pair into the perfect hexagon bonding pattern to connect carbon tubules [10]. The construction based on the C_{60}, and local topological structures of positive and negative Gaussian curvature were obtained theoretically in reference [11]. Haddon provided theoretical investigation on the electron properties of TCN C_{576}, and revealed the quantum nature of quasi-one-dimensional ring [12]. Martel et al. have fabricated rings from SWCNs, and they have observed magnetoresistance at low temperature [13]. The persistent current in TCN was investigated to exhibit novel properties due to the modification of energy structure and energy gap of TCN by applying the magnetic field [14]. TCN can also be used as functional electronic devices, such as the switching and interference devices. The conductance of such a device can be controlled by adjusting the magnetic flux through TCN since its energy gap is strongly associated with magnetic flux. Latil et al. have studied the persistent current in carbon nanotube based rings. The case of interacting nanotori, and the self-interacting coiled nanotubes are analyzed. The rings are not really torii in the usual sense, but are formed by small bundles of nanotubes. The ring is closed by means of weakly interacting bonds rather than covalent bonding [15]. The Aharonov-Bohm-like mesoscopic transport through a TCN coupled to normal metallic leads (N-TCN-N), and through a hybrid system with a TCN coupled to normal and superconducting leads (N-TCN-S) have been investigated to show the resonant and Andreev tunneling controlled by the magnetic flux [16].

Usually, an electronic device is operated under an ac electromagnetic field, especially the radio frequency field.

[a] e-mail: zhaohonk@yahoo.com

Therefore, it is interesting to consider the electronic properties induced by the electromagnetic field. The energy gap is modified by the applied ac field, and the ac Stark effect plays an important role in adjusting the electronic feature of the mesoscopic system [17]. Electrons in the ac field perturbed systems absorb and emit photons to form side-band which acts as channels for electron to tunnel [18]. Since the TCN is quantized in both the transverse and longitudinal directions, the special quantization structure causes novel transport behavior. The electronic structure of TCN and external ac field produce compound effect in the mesoscopic transport, and we can obtain novel output characteristics in such systems.

In this paper, we investigate the physical properties of N-TCN-N threaded with an ac magnetic flux. We assume that electrons in TCN are affected by the homogeneous vector potential in the direction along the ring. This vector potential induces a magnetic flux threading through the TCN parallel to the axis of the ring. Electrons in the TCN are driven by the electric field along the ring to form current. This kind of current is the dynamic current caused by the ac magnetic flux and the interference behavior of electrons in the ring. As the TCN is coupled to two metallic leads, the current transporting through the TCN from the leads is determined by the magnetic flux and the source-drain bias. The feature of current depends sensitively on the detailed structure of TCN. We are interested in both the time-averaged and time-dependent tunneling behaviors, such as the time-averaged current, differential conductance, and the time-oscillating current evolution. We employ the nonequilibrium Green's function (NGF) technique to derive transport formulas which exhibit the information of electromagnetic field and structure of TCN. The numerical calculations are performed to reveal the tunneling behaviors at zero-temperature. The tunneling current and differential conductance versus source-drain bias, magnetic flux, and time are calculated. We make the comparison between the systems in the presence and absence of ac magnetic flux. We present the formalism and derivation of tunneling current in Section 2, and the numerical calculations in Section 3. The concluding remarks are given in Section 4.

2 Model and formalism

The system is composed of three parts: the right and left normal metallic leads, and the central TCN. The TCN is formed by rolling a finite graphite sheet from the origin to the vectors $\mathbf{R}_{\mathrm{x}} = \mathrm{m}_1\mathbf{a}_1 + \mathrm{m}_2\mathbf{a}_2$, and $\mathbf{R}_{\mathbf{y}} = \mathrm{p}_1\mathbf{a}_1 + \mathrm{p}_2\mathbf{a}_2$ simultaneously, where the primitive lattice vectors of the graphite $\mathbf{a}_1$ and $\mathbf{a}_2$ are defined as $\mathbf{a}_1 = (3^{1/2}\mathrm{a}/2, -\mathrm{a}/2)$ and $\mathbf{a}_2 = (3^{1/2}\mathrm{a}/2, \mathrm{a}/2)$ in the $(\mathbf{e}_{\mathrm{x}}, \mathbf{e}_{\mathrm{y}})$ coordinates. The two primitive lattice vectors possess the same magnitude as $a = \mid \mathbf{a}_1 \mid = \mid \mathbf{a}_2 \mid = \mathrm{b} \times 3^{1/2}$, where $b = 1.44$ Å is the C-C bond length of CNs known to be slightly larger than that of graphite [19]. The TCN is denoted by $(m_1, m_2; p_1, p_2)$ as convention, and it satisfies the periodic boundary conditions along both of the longitudinal and transverse directions. We specify that $\mathbf{R}_{\mathrm{x}}$ is in the transverse direction and $\mathbf{R}_{\mathbf{y}}$ in the longitudinal direction. A time-dependent magnetic flux $\tilde{\phi}(t) = \phi + \phi_1 \sin(\omega t)$ is threading through the TCN parallel to its axis $\mathbf{e}_{\mathrm{z}}$, where ϕ is a time-independent magnetic flux, ϕ_1 is the magnitude of ac flux component, and ω is the angular frequency. In the rotating coordinate system with the base vectors $(\mathbf{e}_{\mathrm{r}}, \mathbf{e}_\theta, \mathbf{e}_{\mathrm{z}})$, the time-dependent magnetic flux $\tilde{\phi}(t)$ is induced by the spatially homogeneous electromagnetic vector potential $\mathbf{A}(\mathrm{t})$ in the $\mathbf{e}_\theta$ direction, i.e., $\mathbf{A}(\mathrm{t}) = (\mathrm{A_r}, \mathrm{A}_\theta, \mathrm{A_z})$, with $A_r = 0, A_z = 0$, and $A_\theta = A_0 + A_\omega \sin(\omega t)$. This kind of vector potential can be realized by applying the time-dependent magnetic field in the $\mathbf{e}_{\mathrm{z}}$ direction as $\mathbf{B}(\mathrm{t}) = \mathrm{A}_\theta \mathbf{e}_{\mathrm{z}}/\mathrm{r}$, where r is the distance of the field pointing from the z-axis. We denote the diameter of CN as d_t, and the diameter of mesoscopic ring as D_t. Two kinds of TCN with highly symmetric structures are armchair $(m, m; -p, p)$ TCN and zigzag $(m, 0; -p, 2p)$ TCN. The armchair TCN possesses the symmetry with armchair structure along the transverse direction and zigzag structure along the longitudinal direction. The zigzag TCN has the structure in both of the directions being zigzag. The diameters of the armchair TCN are $d_t = 3bm/\pi$, and $D_t = 3^{1/2}bp/\pi$, and the diameters of the zigzag TCN are given by $d_t = 3^{1/3}bm/\pi$, and $D_t = 3bp/\pi$. In the absence of electromagnetic flux, the armchair TCN is a metal when $p = 3\nu$ (type I TCN), while it is a semiconductor with narrow energy gap as $p = 3\nu \pm 1$ (type II TCN), where ν is an integer. For the zigzag TCN in the absence of electromagnetic flux, there exists a large energy gap when $m \neq 3\nu$ (type III TCN) [14]. We consider the situation that the leads broaden immediately at the connections to the TCN, and the leads are large enough to be considered as equilibrium electron reservoirs. The diameter ratio of the nanotube d_t to the diameter D_t of mesoscopic ring is much smaller than 1, i.e., $\kappa = d_t/D_t \ll 1$. We assume that the TCN is well coupled to the normal metal leads shown as in Figure 1. This geometry of system implies the well coupling of the energy levels of electron in the TCN to the leads. It also signifies that the wave-functions resided in the inner and outer circumferences of TCN roughly couple to the leads equally. The tight-binding model is employed for calculating electron transport through the CN systems where the Coulomb interaction is neglected [20,21]. The tight-binding calculation is relatively simple compared with the first principles

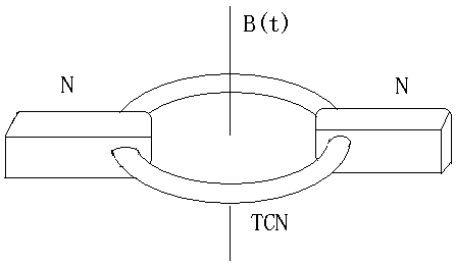

Fig. 1. The schematic diagram of a TCN coupled to two normal metal leads N. The TCN is embedded in the two leads indicating the well coupling of the energy levels of electron in the TCN to the leads.

calculation [22]. On the other hand, the theoretical prediction [23,24] of Luttinger liquid behavior in a SWCN at low energy scale has been verified in the transport experiment [25]. However, the tight-binding calculation can provide main properties of CN systems, such as the electron structure, local density of state, and electron transport. Many scanning tunneling spectroscopic results are fully interpreted in terms of independent electrons model [26]. We are interested in the mesoscopic transport through the TCN systems responded by an external ac field. We take the tight-binding approximation to describe the TCN by avoiding the complexity of involving the Coulomb interaction.

The central TCN is described by the tight-binding Hamiltonian, and the two normal metal leads are described by the free electron grand canonical ensembles. In the diagonalized representation of TCN, the electronic properties can be determined by the total Hamiltonian of the system which is the summation of the three sub-Hamiltonians and the tunneling interaction term

$$H = \sum_{\gamma k\sigma} \epsilon_{\gamma k} a^{\dagger}_{\gamma,k\sigma} a_{\gamma,k\sigma} + \sum_{j\ell\delta\sigma} E_{\ell j,\delta}(t) c^{\dagger}_{\delta\sigma,j\ell} c_{\delta\sigma,j\ell} + \sum_{\gamma k\sigma}\sum_{j\ell\delta} [R^{*}_{\gamma\delta,j\ell}(k) c^{\dagger}_{\delta\sigma,j\ell} a_{\gamma,k\sigma} + \text{h.c.}], \quad (1)$$

where $a^{\dagger}_{\gamma,k\sigma}$ ($a_{\gamma,k\sigma}$), and $c^{\dagger}_{\delta\sigma,j\ell}$ ($c_{\delta\sigma,j\ell}$) are the creation (annihilation) operators of electron in the two leads and TCN, respectively, with $\gamma \in \{L, R\}$. $R_{\gamma\delta,j\ell}(k)$ is interaction strength of electrons between the γth lead and TCN. We take the chemical potential of the right lead as the reference of energy measurement to ensure $\mu_L - \mu_R = eV$, where V is the voltage between the two leads. The spin σ has the values as $\sigma = +1$, and -1 corresponding to the notations $\uparrow$ and $\downarrow$ respectively in the subscripts of equations. $E_{\ell j,\delta}(t)$ is the energy of the TCN. The energy of TCN is intimately associated with the structure of the TCN. However, in the presence of ac magnetic flux, the energy oscillates with external magnetic flux $\tilde{\phi}(t)$. The time-dependent energy can be derived by making gauge transformation and by employing the periodic boundary condition. The time-dependent energy of the armchair TCN can be found in the tight-binding approximation as

$$E_{\ell j,\delta}(t) = \delta\gamma_0 \left\{ 1 + 4\cos^2[\beta_\ell(t)] + 4\cos[\beta_\ell(t)] \cos\left(\frac{j\pi}{m}\right) \right\}^{1/2}. \quad (2)$$

The time-dependent energy of zigzag TCN is given similarly by taking tight-binding approximation

$$E_{\ell j,\delta}(t) = \delta\gamma_0 \left\{ 1 + 4\cos^2\left(\frac{j\pi}{m}\right) + 4\cos[\beta_\ell(t)] \cos\left(\frac{j\pi}{m}\right) \right\}^{1/2}. \quad (3)$$

In the energy formulas (2) and (3), $\beta_\ell(t) = \pi(\ell + \tilde{\phi}(t)/\phi_0)/p$, where $j = 1, 2, ..., m; \ell = 1, 2, ..., 2p; \delta = \pm$, $\gamma_0 = 3.033$ eV, and $\phi_0 = h/e$ is the flux quantum. j and ℓ are the quantum numbers of energy describing the transverse and longitudinal quantization of the TCN, respectively. The upper half of the energy dispersion curves describes the π^*-energy anti-bonding band (unoccupied state), and the lower half of the energy dispersion curves is the π-energy bonding band (occupied state).

The time-dependent retarded Green's function of the isolated TCN in the response of ac flux is defined by

$$g^{r}_{\delta j\ell}(t,t') = -\frac{i}{\hbar}\theta(t-t') \exp\left\{ -\frac{i}{\hbar}\int_{t'}^{t} E_{\ell j,\delta}(\tau) d\tau \right\}. \quad (4)$$

This Green's function depends on both t and t', and it can not be written as the form of time difference in general. However, it can be expressed by

$$g^{r}_{\delta j\ell}(t,t') = -\frac{i}{\hbar}\theta(t-t') \sum_{mn} F^{(mn)}_{\ell j,\delta}(\phi,\phi_1) \times \exp\left\{ -\frac{i}{\hbar}\varepsilon_{\ell j,\delta}(\phi,\phi_1)(t-t') - i(nt-mt')\omega \right\}, \quad (5)$$

(for $n, m = 0, \pm 1 \pm 2, ...$), where $\varepsilon_{\ell j,\delta}$ is the quasi-energy of TCN defined by taking the time average in the period T over the energy $E_{\ell j,\delta}(\tau)$ as

$$\varepsilon_{\ell j,\delta}(\phi,\phi_1) = \frac{1}{T}\int_0^T E_{\ell j,\delta}(\tau) d\tau. \quad (6)$$

The function $F^{(mn)}_{\ell j,\delta}$ is defined by the two-time Fourier transformation as

$$\exp\{-\frac{i}{\hbar}\int_{t'}^{t} [E_{\ell j,\delta}(\tau) - \varepsilon_{\ell j,\delta}(\phi,\phi_1)] d\tau\} = \sum_{mn} F^{(mn)}_{\ell j,\delta}(\phi,\phi_1) \exp[-i(nt-mt')\omega]. \quad (7)$$

Expanding the time-dependent energy formulas given in equations (2, 3) around the time-averaged quasi-energy $\varepsilon_{\ell j,\delta}(\phi,\phi_1)$ to the first-order approximation, and employing the relation

$$\exp[\pm i\Lambda\cos(\omega t)] = \sum_n (\pm i)^n J_n(\Lambda) \exp(\pm in\omega t), \quad (8)$$

we obtain the leading terms of $F^{(mn)}_{\ell j,\delta}$ for the TCNs. In fact, they can be determined by the Bessel function of the first kind $J_n(\Lambda)$ as

$$F^{(mn)}_{\ell j,\delta}(\phi,\phi_1) = (-1)^n i^{n+m} J_n[\Lambda_{\ell j,\delta}(\phi,\phi_1)] J_m[\Lambda_{\ell j,\delta}(\phi,\phi_1)]. \quad (9)$$

The argument of the Bessel function $\Lambda_{\ell j,\delta}(\phi,\phi_1)$ is associated with the detailed structure of TCN. For the armchair TCN, we have the argument of Bessel function

$$\Lambda_{\ell j,\delta}(\phi,\phi_1) = \delta\frac{4\gamma_0}{\hbar\omega} J_1(\alpha_1) \left[\cos\left(\frac{\pi j}{m}\right) \sin(\beta_\ell) + J_0(\alpha_1) \sin(2\beta_\ell) \right],$$

and for the zigzag TCN, we obtain the argument of Bessel function as

$$\Lambda_{\ell j,\delta}(\phi,\phi_1) = \delta\frac{4\gamma_0}{\hbar\omega}J_1(\alpha_1)\cos\left(\frac{\pi j}{m}\right)\sin(\beta_\ell),$$

where $\beta_\ell = \pi(\ell+\phi/\phi_0)/p$, and $\alpha_1 = \pi\phi_1/p\phi_0$. The function $F^{(mn)}_{\ell j,\delta}$ modifies the magnitude of tunneling current in each channel of the quantum system in the presence of ac flux. This reveals additional feature of the mesoscopic transport, which is strongly associated with the structure of central region. As $\alpha_1 \to 0$, $F^{(mn)}_{\ell j,\delta} \to 1$, which is the situation in the absence of ac flux.

The mesoscopic transport under the ac fields can be derived by NGF technique, and the detailed derivation of current formula can be found in references [27–29]. The time-dependent tunneling current of the γth lead is determined by the current formula

$$I_\gamma(t) = 2eRe\sum_{\delta j\ell\sigma}\int dt_1[G^r_{\delta j\ell}(t,t_1)\Sigma^<_{\gamma,\delta j\ell}(t_1,t) + G^<_{\delta j\ell}(t,t_1)\Sigma^a_{\gamma,\delta j\ell}(t_1,t)], \quad (10)$$

where $\Sigma^X_{\gamma,\delta j\ell}(t_1,t_2)$ is the self-energy of the γth lead defined by $\Sigma^X_{\gamma,\delta j\ell}(t,t') = \sum_k \mid R_{\gamma\delta,j\ell} \mid^2 g^X_{\gamma,k\sigma}(t,t')$, ($X \in \{r,a,<\}$). In the self-energy, $g^X_{\gamma,k\sigma}(t,t')$ is the Green's function of the γth lead.

The time-dependent Green's function of the coupled TCN can be expanded by

$$G^X_{\delta j\ell}(t,t') = \sum_{mn} F^{(mn)}_{\ell j,\delta}(\phi,\phi_1)e^{-i\omega(nt-mt')}\tilde{G}^X_{\delta j\ell}(t,t'). \quad (11)$$

Here the Green's function $\tilde{G}^X_{\delta j\ell}(t,t')$ is associated with the system in the absence of ac flux. The retarded Green's function is determined by the Dyson equation

$$\tilde{G}^r_{\delta j\ell}(t,t') = \tilde{g}^r_{\delta j\ell}(t,t') + \iint dt_1dt_2\tilde{g}^r_{\delta j\ell}(t,t_1) \times \Sigma^r_{\delta j\ell}(t_1,t_2)\tilde{G}^r_{\delta j\ell}(t_2,t'), \quad (12)$$

where $\tilde{g}^r_{\delta j\ell}(t,t')$ is the retarded Green's function of the isolated TCN in the absence of ac flux. The Keldysh Green's function of the coupled TCN is given by the equation [27]

$$\tilde{G}^<_{\delta j\ell}(t,t') = \iint dt_1dt_2\tilde{G}^r_{\delta j\ell}(t,t_1) \times \Sigma^<_{\delta j\ell}(t_1,t_2)\tilde{G}^a_{\delta j\ell}(t_2,t'). \quad (13)$$

The self-energy above is defined by summing the self-energies of the leads as $\Sigma^X_{\delta j\ell}(t_1,t_2) = \sum_\gamma \Sigma^X_{\gamma,\delta j\ell}(t_1,t_2)$.

2.1 Time-averaged mesoscopic transport

The time-averaged tunneling current is related to the Green's function of the TCN expressed by the pseudo-equilibrium state. For this situation, the diagonal elements of the function $F^{(nm)}_{\ell j,\delta} = F^{(n)}_{\ell j,\delta} = J^2_n[\Lambda_{\ell j,\delta}(\phi,\phi_1)]$ (for $m=n$) contribute to the Green's function

$$g^r_{\delta j\ell}(t,t') = -\frac{i}{\hbar}\theta(t-t')\sum_n F^{(n)}_{\ell j,\delta}(\phi,\phi_1) \times \exp\left\{-\frac{i}{\hbar}[\varepsilon_{\ell j,\delta}(\phi,\phi_1)+n\hbar\omega](t-t')\right\}. \quad (14)$$

The Fourier transformed version of the Green's function above is then expressed as

$$g^r_{\delta j\ell}(\epsilon) = \sum_n F^{(n)}_{\ell j,\delta}(\phi,\phi_1)\tilde{g}^r_{\delta j\ell}(\epsilon-n\hbar\omega), \quad (15)$$

where $\tilde{g}^r_{\delta j\ell}(\epsilon)$ is the Fourier transformation defined by

$$\tilde{g}^r_{\delta j\ell}(\epsilon) = \frac{1}{\epsilon-\varepsilon_{\ell j,\delta}(\phi,\phi_1)+i\eta}. \quad (16)$$

with $\eta \to 0$. The tunneling current formula can be derived from the Heisenberg equation and continuity equation by employing the NGF technique. The time-averaged current in the γth lead can be expressed as the Landauer-Büttiker-like formula [30]

$$I_\gamma = \frac{e}{h}\sum_{n\sigma}\sum_{\gamma\neq\beta}\int d\epsilon T_{\gamma\beta,n}(\epsilon)[f_\gamma(\epsilon)-f_\beta(\epsilon)], \quad (17)$$

where $T_{\gamma\beta,n}(\epsilon) = \sum_{\ell j\delta}\Gamma_{\gamma,\delta j\ell}(\epsilon)\Gamma_{\beta,\delta j\ell}(\epsilon)F^{(n)}_{\ell j,\delta}(\phi,\phi_1) \times |\tilde{G}^r_{\delta j\ell}(\epsilon-n\hbar\omega)|^2$ is the transmission coefficient representing the electron tunneling from the γth lead to the βth lead. It possesses the symmetry property about leads as $T_{\gamma\beta}(\epsilon) = T_{\beta\gamma}(\epsilon)$. This means that the electron transporting from the βth lead to the γth lead is equal to the transporting from the γth lead to the βth lead. $\Gamma_{\gamma,\delta j\ell}(\epsilon)$ is the line-width defined by $\Gamma_{\gamma,\delta j\ell}(\epsilon) = 2\pi\sum_k \mid R_{\gamma\delta,j\ell} \mid^2 \delta(\epsilon-\epsilon_{\gamma k})$. The function $f_\gamma(\epsilon)$ is the Fermi distribution function of the γth lead. We consider the wide-band limit for the leads, which means that the line-widths are independent on the energy levels. For this situation, $\Gamma_{\gamma,\delta j\ell}(\epsilon) = \Gamma_\gamma$, and $\tilde{G}^r_{\delta j\ell}(\epsilon)$ is the pseudo-equilibrium retarded Green's function of the coupled TCN determined by

$$\tilde{G}^r_{\delta j\ell}(\epsilon) = \frac{1}{\epsilon-\varepsilon_{\ell j,\delta}(\phi,\phi_1)+i\Gamma}. \quad (18)$$

where $\Gamma = (\Gamma_L+\Gamma_R)/2$.

The electron band structure and transport property of this TCN system are mainly determined by the π valence electrons. Tight-binding calculation for the π electrons is proven to be in good agreement with experiment. It can provide important insights for understanding the electronic structure of π energy level in the CN system. As the external electromagnetic field is applied to the system, the energy spectrum is modified considerably. By taking time-average over the time-dependent energy from equation (6), the calculation reveals that the quasi-energy of the armchair TCN in the tight-binding approximation is

given as [17]

$$\varepsilon_{\ell j,\delta}(\phi,\phi_1)=\delta\gamma_0\Bigg\{1+4\sum_{n=-\infty}^{\infty}\big[J_{2n}^2(\alpha_1)\cos^2(\beta_\ell) + J_{2n+1}^2(\alpha_1)\sin^2(\beta_\ell)\big]+4J_0(\alpha_1)\cos(\beta_\ell)\cos\left(\frac{j\pi}{m}\right)\Bigg\}^{1/2}. \quad (19)$$

The quasi-energy of the zigzag TCN is given similarly by taking tight-binding approximation

$$\varepsilon_{\ell j,\delta}(\phi,\phi_1)=\delta\gamma_0\Bigg\{1+4\cos^2\left(\frac{j\pi}{m}\right) + 4J_0(\alpha_1)\cos(\beta_\ell)\cos\left(\frac{j\pi}{m}\right)\Bigg\}^{1/2}. \quad (20)$$

In equations (19, 20), $\beta_\ell=\pi(\ell+\phi/\phi_0)/p$, $\alpha_1=\pi\phi_1/p\phi_0$, where $j=1,2,...,m;\ell=1,2,...,2p$. We have denoted that $\delta=\pm$, which indicates the upper half and lower half of the energy dispersion curves. The highest occupied state and the lowest unoccupied state meet with each other at the Fermi energy E_F in the absence of external magnetic field for the armchair type I TCN, while it possesses a small energy gap for the type II TCN. Due to the symmetric structure, the Fermi energy is located at $E_F=0$. As the external electromagnetic field is applied to the TCN, the energy gap changes, and it is intimately related to the magnitude of field. Obviously, the quasi-energy formulas equations (19, 20) reduce to the energy formulas of TCN given in reference (14) by letting $\alpha_1\to 0$. This can be seen by noticing that $J_n(0)=\delta_{n0}$.

We take the potential of right lead as the reference by setting $\mu_R=0$ in the formula. At zero temperature, the tunneling current formula (17) is reduced to

$$I=\frac{e}{h}\sum_\sigma\int_0^{eV}T_{LR}(\epsilon)d\epsilon, \quad (21)$$

where the transmission coefficient $T_{LR}(\epsilon)$ is defined as

$$T_{LR}(\epsilon)=\sum_{\delta\ell jn}\frac{\Gamma_L\Gamma_R F_{\ell j,\delta}^{(n)}(\phi,\phi_1)}{[\epsilon-\varepsilon_{\ell j,\delta}(\phi,\phi_1)-n\hbar\omega]^2+\Gamma^2}. \quad (22)$$

$T_{LR}(\epsilon)$ is the transmission coefficient of electrons transporting from the right to the left lead. It is the contribution of electrons tunneling through all of the channels in the TCN. The electrodes are considered to be large electron reservoirs which provide the possibility for electrons to meet the transport through each of the channels. The applied ac magnetic flux induces side-band due to the absorption and emission of photons. The central TCN acts as a scattering center, and the Breit-Wigner resonant transport takes place as $\epsilon-\varepsilon_{\ell j,\delta}(\phi,\phi_1)-n\hbar\omega=0$. The evidence for the resonant transmissions has been observed experimentally in SWCN system [3].

2.2 The time-dependent mesoscopic transport

In this subsection, we study the time-dependent mesoscopic transport through the N-TCN-N system. We make Fourier transformation over the time-dependent current formula equation (10) to give the tunneling current of the γth lead

$$I_\gamma(t)=2eRe\sum_{\delta j\ell\sigma}\left(\frac{1}{2\pi\hbar}\right)^2\int d\epsilon_1 d\epsilon_2\exp\left[-\frac{i}{\hbar}(\epsilon_1-\epsilon_2)t\right] \times[G^r_{\delta j\ell}(\epsilon_1,\epsilon_2)\Sigma^<_{\gamma,\delta j\ell}(\epsilon_2)+G^<_{\delta j\ell}(\epsilon_1,\epsilon_2)\Sigma^a_{\gamma,\delta j\ell}(\epsilon_2)], \quad (23)$$

where $G^X_{\delta j\ell}(\epsilon_1,\epsilon_2)$ and $\Sigma^X_{\delta j\ell}(\epsilon_2)$ are the Green's function and self-energy in the energy representation. The self-energy is determined by the Green's functions of the leads as $\Sigma^X_{\gamma,\delta j\ell}(\epsilon)=\sum_k\mid R_{\gamma\delta,j\ell}\mid^2 g^X_{\gamma,k\sigma}(\epsilon)$, $(X\in\{r,a,<\})$, where $g^{r(a)}_{\gamma,k\sigma}(\epsilon)=1/(\epsilon-\epsilon_{\gamma k}\pm i\eta)$, $(\eta\to 0)$, and the Keldysh Green's function is $g^<_{\gamma,k\sigma}(\epsilon)=2\pi i f_\gamma(\epsilon)\delta(\epsilon-\epsilon_{\gamma k})$.

The time-dependent tunneling current expression equation (10) now becomes

$$I_\gamma(t)=-2eIm\sum_{\delta j\ell\sigma}\left(\frac{1}{2\pi\hbar}\right)^2\int d\epsilon_1 d\epsilon_2\exp\left[-\frac{i}{\hbar}(\epsilon_1-\epsilon_2)t\right] \times\Gamma_{\gamma,\delta j\ell}(\epsilon_2)\left[G^r_{\delta j\ell}(\epsilon_1,\epsilon_2)f_\gamma(\epsilon_2)+\frac{1}{2}G^<_{\delta j\ell}(\epsilon_1,\epsilon_2)\right]. \quad (24)$$

The Dyson equation for the retarded Green's function in the energy representation is obtained from equation (12)

$$\tilde{G}^r_{\delta j\ell}(\epsilon,\epsilon')=\tilde{g}^r_{\delta j\ell}(\epsilon,\epsilon')+\frac{1}{2\pi\hbar}\int d\epsilon_1\tilde{g}^r_{\delta j\ell}(\epsilon,\epsilon_1) \times\Sigma^r_{\delta j\ell}(\epsilon_1)\tilde{G}^r_{\delta j\ell}(\epsilon_1,\epsilon'). \quad (25)$$

By making Fourier transformation over equation (11), the Green's function of the TCN in the presence of ac flux can be expressed by the expansion of $\tilde{G}^r_{\delta j\ell}(\epsilon)$ as

$$G^X_{\delta j\ell}(\epsilon,\epsilon')=2\pi\hbar\sum_{mn}F^{(mn)}_{\ell j,\delta}(\phi,\phi_1)\tilde{G}^X_{\delta j\ell}(\epsilon-n\hbar\omega) \times\delta[\epsilon-\epsilon'-(n-m)\hbar\omega], \quad (26)$$

for $X\in\{r,a,<\}$. The Fourier transformed Keldysh Green's function in equation (26) is

$$\tilde{G}^<_{\delta j\ell}(\epsilon-n\hbar\omega)=\Sigma^<_{\delta j\ell}(\epsilon)\mid\tilde{G}^r_{\delta j\ell}(\epsilon-n\hbar\omega)\mid^2. \quad (27)$$

We consider the wide-band limit for the leads such that the self-energies $\Sigma^{r(a)}_{\delta j\ell}(\epsilon)=\mp i\sum_\gamma\Gamma_\gamma/2$, and $\Sigma^<_{\delta j\ell}(\epsilon)=i\sum_\gamma\Gamma_\gamma f_\gamma(\epsilon)$. We are interested in the time-oscillating tunneling current induced by the ac flux for general V. Obviously, when $V=0$, the time averaged current is zero from equation (21). The retarded Green's function $\tilde{G}^r_{\delta j\ell}(\epsilon)$ is given by equation (18).

Substituting the Green's functions given in equation (26) and wide-band limit self-energies into equation (24), we immediately obtain the time-dependent tunneling current in the presence of source-drain bias as

$$I_\gamma(t) = \frac{e}{h}\sum_{\delta j\ell\sigma}\sum_{mn}\tilde{F}^{(mn)}_{\ell j,\delta}(\phi,\phi_1)\{I^{(1)}_{\gamma,mn}\cos[W_{nm}(t)] + I^{(2)}_{\gamma,mn}\sin[W_{nm}(t)]\}, \quad (28)$$

where $W_{nm}(t) = (n-m)\omega t - (n+m)\pi/2$ and $I^{(1)}_{\gamma,mn}$ and $I^{(2)}_{\gamma,mn}$ are defined as

$$I^{(1)}_{\gamma,mn} = \sum_{\gamma'}\int d\epsilon \Gamma_\gamma\Gamma_{\gamma'} \mid \tilde{G}^r_{\delta j\ell}(\epsilon - n\hbar\omega) \mid^2 \times \{f_\gamma[\epsilon + (m-n)\hbar\omega] - f_{\gamma'}(\epsilon)\},$$

$$I^{(2)}_{\gamma,mn} = 2\Gamma_\gamma\int d\epsilon Re\tilde{G}^r_{\delta j\ell}(\epsilon - n\hbar\omega) f_\gamma[\epsilon + (m-n)\hbar\omega].$$

In equation (28), we have defined the relation $F^{(mn)}_{\ell j,\delta} = i^{n+m}\tilde{F}^{(mn)}_{\ell j,\delta}$. The time-averaged tunneling current given in equation (17) corresponds to the case $m = n$ in equation (28). One observes that although the time-averaged tunneling current is zero when $V = 0$, we can have time-oscillating current induced by the ac flux. However, the tunneling current depends on the detailed structure of the TCN and the applied magnetic field.

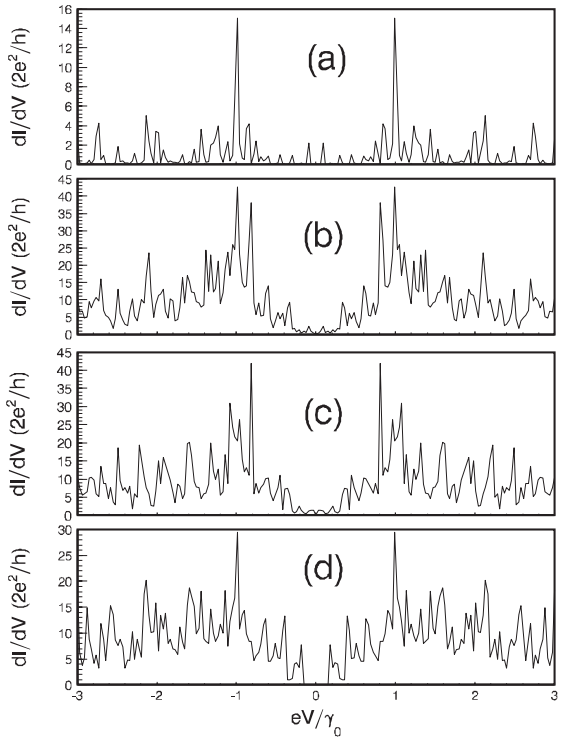

Fig. 2. The differential conductance dI/dV versus source-drain bias eV at zero temperature for $\phi = 0, \alpha_1 = 0.01, \hbar\omega = 0.01\gamma_0$. Diagrams (a), (b) (c) and (d) are associated with the type I $(5,5;-120,120)$, $(10,10;-480,480)$, type II $(10,10;-481,481)$ and type III $(10,0;-480,960)$ TCNs, respectively.

3 Numerical calculation

In this section, we perform the numerical calculations on the tunneling current in the presence of ac magnetic flux at zero temperature. Defining $\Omega = \phi_0/3^{1/2}\pi b = 5.3\times10^{-4}$ T m, the dimensionless quantity α_1 can be expressed as $\alpha_1 = A_\omega/\Omega$. The energy is an periodic function of ϕ, and its magnitude depends on the magnitude of ac field. In the numerical calculations, we take $G_0 = 2e^2/h$ as the measurement scale of conductance, and $I_0 = 2e\gamma_0/h = 2.35\times10^{-4}$ A as the scale of tunneling current. We consider the symmetric situation where the two leads are composed of the same material, and they are equally coupled to the quantum TCN. So that the line-widths are equal and energy independent. The equally coupled symmetric system is considered by choosing $\Gamma_L = \Gamma_R = 0.001\gamma_0$. The frequency is scaled by the quantity $\gamma_0/h = 7.36\times10^{14}$ Hz.

The differential conductance dI/dV at zero temperature is given directly from equation (21) that

$$\frac{dI}{dV} = \frac{e^2}{h}\sum_\sigma T_{LR}(eV). \quad (29)$$

Figure 2 is the differential conductance versus the source-drain bias eV. The bias eV is scaled by γ_0, which corresponds to 3.033V source-drain voltage. The frequency of ac magnetic flux is $f = 7.36\times10^{12}$ Hz, which is in the order of tera hertz. In the absence of ac component magnetic flux, i.e., $\phi_1 = 0$, the metal-semiconductor phase transition takes place in the type I and II TCNs by varying dc magnetic flux ϕ which has been documented in the literatures [14,16,31,32]. The type III TCN is always semiconductor with energy gap $E \approx 1.0$ eV. The energy gaps increase with increasing the ac magnetic flux ϕ_1. In the absence of magnetic flux, the energy gaps of type I materials in Figures 2a and b are zero $E_g = 0$. The energy gaps of the type II TCN in Figure 2c and type III TCN in Figure 2d are about $E_g \approx 48$ meV, and 1.0 eV, respectively. As the ac magnetic flux is applied, the energy gaps increase due to the two components of magnetic flux ϕ and ϕ_1. The photon energy with tera hertz frequency $f = 7.36\times10^{12}$ Hz is about 30 meV. If the magnitude of ac flux is small enough, i.e., $\alpha_1 \ll 1$, the energy gap of armchair TCN is small. The zero-biased conductance is small, but it becomes large by applying nonzero bias voltage. There may exist tunneling current as $eV \neq 0$ by absorbing enough photons. For the type III TCN one observes that the energy gap is large $E_g \approx 1.0$ eV. For such material, the valence electron can not jump to the conductance band by absorbing the photon energy with tera hertz frequency. The resonant peaks reflect the discrete energy levels in the TCNs, and the level spacings reduce as the TCNs become large. As the ac flux is applied, some

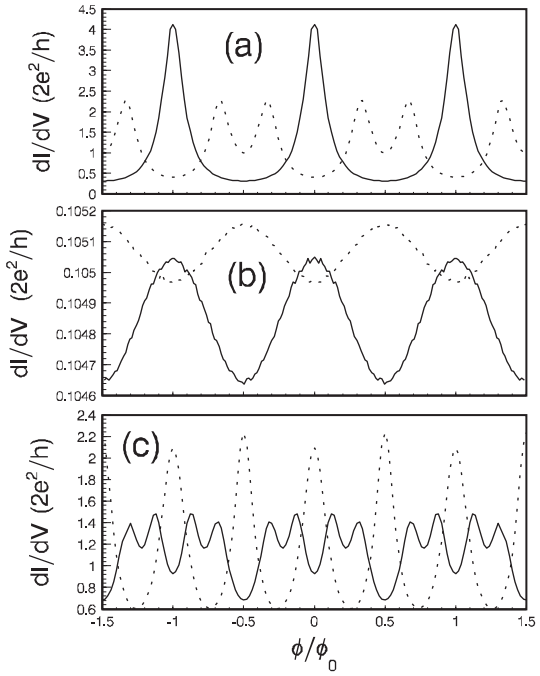

Fig. 3. The differential conductance dI/dV versus dc magnetic flux ϕ at zero temperature. Diagram (a) is the conductance oscillation of TCNs when $\alpha_1 = 0$ and $eV = 0$ for $(10, 10; -480, 480)$ (the solid curve) and $(10, 10; -481, 481)$ (the dotted curve). Diagram (b) is the conductance of TCNs when $\alpha_1 = 0.01, \hbar\omega = 0.01\gamma_0$ and $eV = 0$. The solid and dotted curves are associated with $(10, 10; -480, 480)$ and $(10, 10; -481, 481)$ TCNs, respectively. Diagram (c) is associated with the case for $\alpha_1 = 0$ and the source-drain voltage $V = 0.61$ volt. The solid and dotted curves are related to the type I $(10, 10; -480, 480)$ and type II $(10, 10; -481, 481)$ TCNs, respectively.

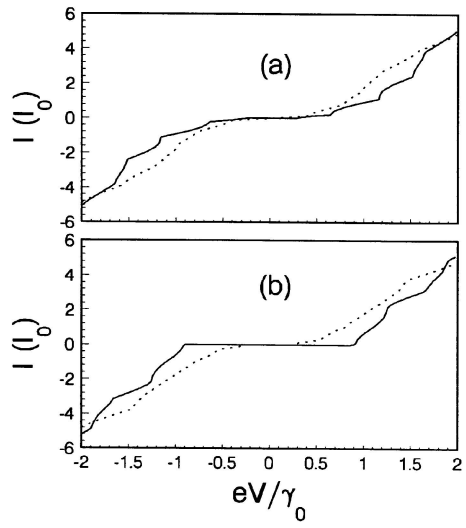

Fig. 4. The I-V characteristics of TCN with applied ac flux as $\phi = 0$. The dotted and solid curves are associated with $\alpha_1 = 0$ and $\alpha_1 = 3.8317$, respectively. Diagrams (a) and (b) correspond to the systems associated with (7,7;160,160) and $(7, 0; -160, 320)$ TCNs.

of the resonant peaks are suppressed, and some of them are enhanced to form photon-assisted resonant structure.

Figure 3 displays the zero-biased and source-drain biased differential conductance versus dc magnetic flux ϕ at zero temperature. The zero-biased conductance is strongly dependent on the ac flux. However, the conductance oscillation versus dc magnetic flux ϕ exhibits the symmetric and periodic properties $G(\phi) = G(-\phi)$ and $G(\phi) = G(\phi + n\phi_0)$, $(n = 0, \pm1, \pm2, ...)$. For the type I TCN as $\alpha_1 = 0$, the zero-biased conductance resonates at $\phi = n\phi_0$, where the metal-semiconductor phase transition takes place. Away from these transition points, the conductance declines with the minimum value $G = 0.3G_0$. For the type II TCN, the resonances of $G(\phi)$ occur at $\phi = (1/3 + n)\phi_0, (2/3 + n)\phi_0$, where the metal-semiconductor phase transition takes place (diagram (a)). This indicates that the Aharonov-Bohm magnetic flux controls the conductance from metal to semiconductor changes periodically, and different types of TCN possess different transport behavior. In the semiconductor regimes, we also have nonzero conductance, however it is small. As the ac flux is applied, one observes that the conductance is very small, and the oscillation behavior is similar for type I TCN as the case for $\alpha_1 = 0$, but it is quite different for the type II TCN as the case for $\alpha_1 = 0$ (diagram (b)). The two peaks in a period of type II TCN unite to form one, and it has $\phi_0/2$ phase difference from that of type I TCN. Since the ac flux component ϕ_1 always increases the energy gap of TCN [17], it is clear that the double-peak oscillation in type II TCN only exists as the energy gap is small. The differential conductance dI/dV versus magnetic flux ϕ at zero temperature in the presence of source-drain bias is given in diagram (c). The dI/dV is sensitive to the applied voltage V and the types of TCN. For the type I TCN, one observes that cluster oscillation takes place, i.e., in one period ϕ_0, there exist 4 peaks located on the main hill, and they are symmetric about the center of the hill.

The transport behavior is strongly dependent on the magnitude α_1 associated with the ac flux, since it makes contribution to the quasi-energy $\varepsilon_{\ell j,\delta}$ and weight function $F^{(n)}_{\ell j,\delta}$. The weight function is determined by the Bessel function $J_n(\Lambda)$ with its variables Λ itself composed of the Bessel function $J_1(\alpha_1)$ (see Eqs. (9)). Therefore, the transmission coefficient becomes very complicated due to the influence of an ac flux. However, when α_1 is the zero of Bessel function $J_1(\alpha_1)$, the transmission coefficient reduces to a very simple expression. The corresponding behavior is obtained by taking $n = 0$, and $F^{(n)}_{\ell j,\delta} \to 1$ in $T_{LR}(\epsilon)$. For this circumstance, the transport behavior is similar to the case when the external ac flux is switched off. However, the ac field still contributes to the quasi-energy through the other Bessel functions. The ac flux increases the energy gap which is obviously seen in Figure 4. Figures 4a and b show the current-voltage characteristics of the type II armchair and type III zigzag TCNs system. As the external ac flux is applied at the zero of $J_1(\alpha)$ with

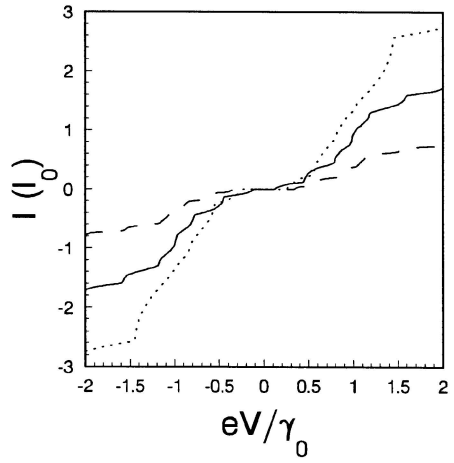

Fig. 5. The I-V characteristics of TCN with applied ac flux when $\phi = 0$ for different α_1. The solid and dashed curves are related to the $(7, 7; -160, 160)$ TCN when $\alpha_1 = 0.1$ and $\alpha_1 = 0.3$, respectively. The dotted curve is associated with $(7, 0; -160, 320)$ TCN for $\alpha_1 = 0.1$.

$\alpha_1 = 3.8317$, the current appears obvious steps, and the threshold increases. The tunneling current of the system in the absence of ac flux is larger than that of the system in the presence of ac flux in region $0 < eV < 1.84\gamma_0$, and an intersection occurs at about $eV = 1.84\gamma_0$.

We show the photon-assisted tunneling versus the source-drain bias in the presence of ac magnetic flux in Figure 5. As the magnitude α_1 increases from 0.1 to 0.3, the magnitude of tunneling current decreases. We also observe that the energy gap is increased by increasing α_1 (the solid and dashed curves). The stair-like structure of the current-voltage characteristics is associated with the emission and absorption of photons. The steps of the current are related to the quantum level of the TCN and sideband caused by photon energy. For the time-averaged tunneling, the effect of the photon absorption and emission is to split the energy level of TCN and modifies the current. The tunneling current resonate with the local electron in the quantum TCN, and with the applied photons. The dotted curve shows the tunneling current of type III TCN as $\alpha_1 = 0.1$. The magnitude of the current is larger than the type II TCN, and the stairs are not obviously observed compared with the type II TCN. The I-V curves are quite different from the ones in the absence of ac component of magnetic flux shown in reference [16]. We can also see that the energy gap E_g increases by applying the ac magnetic flux stated in reference [17].

The tunneling current versus dc magnetic flux ϕ is presented in Figure 6 to show the oscillation and influence of the dc and ac flux components. Diagrams (a), (b) are the tunneling currents through the type II TCN $(7, 7; -160, 160)$ as $\alpha_1 = 0$, and $\alpha_1 = 3.8317$, respectively. Diagrams (c), (d) are the tunneling currents through the type I TCN $(7, 7; -159, 159)$ as $\alpha_1 = 0$, and $\alpha_1 = 3.8317$, respectively. The currents exhibit periodic behaviors with period ϕ_0, but the magnitude of the oscillation and shape structure are different between type I

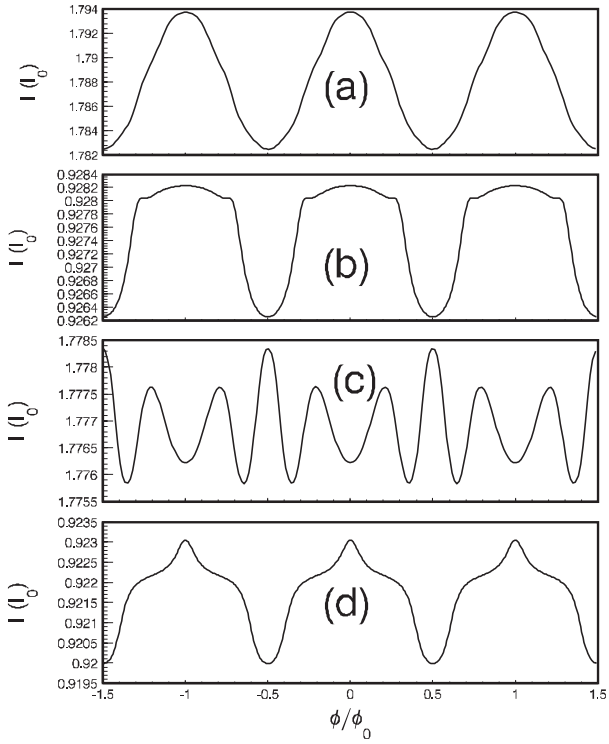

Fig. 6. The tunneling current $I(\phi)$ versus the magnetic flux ϕ at $eV = \gamma_0$. Diagrams (a) and (b) correspond to the $(7, 7; -160, 160)$ TCN with the parameter $\alpha_1 = 0$ and $\alpha_1 = 3.8317$, respectively. Diagrams (c) and (d) correspond to the $(7, 7; -159, 159)$ TCN with the parameter $\alpha_1 = 0$ and $\alpha_1 = 3.8317$, respectively.

and type II TCNs. The magnitude of the current is suppressed by the applied ac flux. This is resulted from the fact that the applied ac field increases the energy gap E_g from the original one of TCN. The tunneling electrons residing in the conductance band for the semiconducting TCN are much less than those in the metallic TCN. The modification of current is associated with the modification of quasi-energy for each TCN. The modification of current by the ac flux is obviously seen for the type I TCN. In the absence of ac flux, the tunneling current oscillates with two kinds of vibration structure. One kind of wave packet is located at $\phi = n\phi_0$, $(n = 0, \pm 1, \pm 2, ...)$, and the other one is located at $\phi = (n+1/2)\phi_0$. As the ac flux is applied, the current oscillation is modified to form only one vibration structure, with the modified wave packets located at $\phi = n\phi_0$.

For the symmetric system, the net tunneling is determined by $I(t) = [I_L(t) - I_R(t)]/2$, because the currents coming out of the quantum TCN are cancelled exactly. Therefore, the net tunneling current is derived as

$$I(t) = \frac{e}{h}\Gamma \sum_{\delta j \ell \sigma} \sum_{mn} \tilde{F}^{(mn)}_{\ell j,\delta}(\phi, \phi_1)\{I^{(1)}_n \cos[W_{nm}(t)] + I^{(2)}_n \sin[W_{nm}(t)]\}, \quad (30)$$

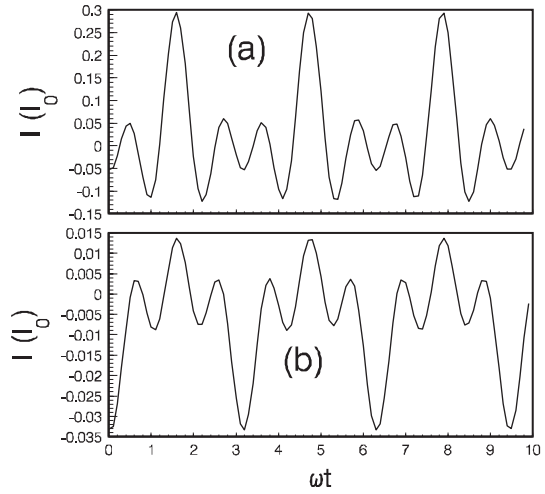

Fig. 7. The time-dependent current evolving periodically with ωt for the $(7,7;-160,160)$ TCN. The parameters are chosen as $eV = 0.8\gamma_0$, $\phi = 0$. Diagrams (a) and (b) are associated with $\alpha_1 = 0.1$ and 0.8, respectively.

where

$$I_n^{(1)} = \tan^{-1}\left[\frac{\mu_R + eV - \varepsilon_{\ell j,\delta}(\phi,\phi_1) - n\hbar\omega}{\Gamma}\right] - \tan^{-1}\left[\frac{\mu_R - \varepsilon_{\ell j,\delta}(\phi,\phi_1) - n\hbar\omega}{\Gamma}\right], \quad (31)$$

$$I_n^{(2)} = \frac{1}{2}\ln\left\{\frac{[\mu_R + eV - \varepsilon_{\ell j,\delta}(\phi,\phi_1) - n\hbar\omega]^2 + \Gamma^2}{[\mu_R - \varepsilon_{\ell j,\delta}(\phi,\phi_1) - n\hbar\omega]^2 + \Gamma^2}\right\}. \quad (32)$$

The time-dependent tunneling current is induced by the ac magnetic flux, and the net current is zero as the source-drain bias is zero for the symmetric system. This can be understood that the pumped current coming out of the central TCN to the two leads are equal as $eV = 0$. The oscillating current evolves periodically with ωt in the period associated with the superposition of oscillation components $(n-m)\omega t$. We depict the time-oscillating current versus ωt in Figure 7 to show the current evolution procedure. The current oscillation structure is observed to have strong relation with the magnitude α_1 of applied ac field. In diagram (a), there exist two kinds of oscillation structure with the same period. A small oscillation with split peaks is embedded in the valleys of the main oscillation with larger single peaks. As α_1 increases, the oscillating current is suppressed, and the oscillating structure changes. Two kinds of oscillation merge to form the time-evolving current with three peaks located on a main peak. The time-dependent current is determined by the resonant levels, the magnitude of the ac flux, and the frequency. As α_1 increases, the energy gap E_g increases, and the weight function $F_{\ell j,\delta}$ makes contribution to the current significantly.

4 Concluding remarks

We have investigated the quantum transport through the N-TCN-N systems threaded by an ac magnetic flux. The tunneling current formula is derived by employing NGF technique. The time-dependent and time-averaged currents are calculated. The frequency-dependent transmission coefficient $T_{\gamma\beta,n}(\epsilon)$ plays the central role for the coherent transport. Because of the perturbation of ac magnetic flux, the transmission coefficient appears very complicated form by involving the field effect in the quasi-energy and the weight function $F_{\ell j,\delta}$. This makes the tunneling behaviors complicated when the electron does not match the quasi-energy of the TCN. The energy shift takes place by applying the magnetic flux, and this shift arises from both the dc and ac components of magnetic flux. The dc magnetic flux ϕ induces the periodic variation of energy gap, and the ac flux component always increases the energy gap. On the other hand, the time-dependent magnetic field produces side-band of quasi-energy, which provides novel channels for electrons to tunnel through. As the photon energy is larger than the energy gap $\hbar\omega > E_g$, the electrons in the valence band can jump to the conductance band at zero temperature, and the tunneling current appears as $eV > E_g/2 + n\hbar\omega$, $(n = 0, \pm1, \pm2, ...)$. The tunneling is very simple for the resonant circumstance as $\epsilon - \varepsilon_{\ell j,\delta}(\phi,\phi_1) - n\hbar\omega = 0$. The transport features are different for different TCN systems as type I, II, and III TCNs. The differential conductance and tunneling current display obvious effect of ac flux by modifying the current oscillation structures. However the modification is quite simple as α_1 is a zero of $J_1(\alpha_1)$. The time-dependent current oscillates periodically with ωt. The detailed evolution structure is the superposition of different components of oscillating current branches. The magnitude of the ac flux ϕ_1 plays an important role for the photon absorption and emission procedure, and it affects the tunneling current considerably. Since the system is controlled by the external magnetic flux, we can adjust the magnitudes of dc and ac components of magnetic flux by varying ϕ, ϕ_1 and ω to obtain desired tunneling current. This system acts as a magnetic flux controlled interference switching device.

This work was supported by a RGC grant from the SAR Government of Hong Kong under Grant No. HKU 7032/03P and by the National Natural Science Foundation of China under the Grant No. 10375007.

References

1. S. Iijima, Nature (London) **354**, 56 (1991)
2. J.W. Mintmire, B.I. Dunlap, C.T. White, Phys. Rev. Lett. **68**, 631 (1992)
3. S.J. Tans, M.H. Devoret, H. Dai, A. Thess, R.E. Smalley, L.J. Geerligs, C. Dekker, Nature (London) **386**, 474 (1997)
4. C. Zhou, J. Kong, H. Dai, Phys. Rev. Lett. **84**, 5604 (2000)
5. T.W. Odom, J.L. Huang, P. Kim, C.M. Lieber, Nature (London) **391**, 62 (1998)
6. S.J. Tans, A.R.M. Verschueren, C. Dekker, Nature (London) **393**, 49 (1998)

7. A. Bachtold, C. Strunk, J.P. Salvetat, J.M. Bonard, L. Forró, T. Nussbaumer, C. Schönenberger, Nature (London) **397**, 673 (1999)
8. Y. Xue, S. Datta, Phys. Rev. Lett. **83**, 4844 (1999)
9. H. Mehrez, J. Taylor, H. Guo, J. Wang, C. Roland, Phys. Rev. Lett. **84**, 2682 (2000); C. Roland, M.B. Nardelli, J. Wang, H. Guo, Phys. Rev. Lett. **84**, 2921 (2000)
10. B.I. Dunlap, Phys. Rev. B **46**, 1933 (1992)
11. S. Itoh, S. Ihara, J. Kitakami, Phys. Rev. B **47**, 1703 (1993); S. Itoh, S. Ihara, J. Kitakami, Phys. Rev. B **47**, 12908 (1993)
12. R.C. Haddon, Nature **388**, 31 (1997)
13. R. Martel, H.R. Shea, Ph. Avouris, Nature (London) **398**, 299 (1999); H.R. Shea, R. Martel, Ph. Avouris, Phys. Rev. Lett. **84**, 4441 (2000)
14. M.F. Lin, D.S. Chuu, Phys. Rev. B **57**, 6731 (1998)
15. S. Latil, S. Rouche, A. Rubio, Phys. Rev. B **67**, 165420 (2003)
16. H.K. Zhao, Phys. Lett. A **308**, 226 (2003); H.K. Zhao, Phys. Lett. A **310**, 207 (2003); H.K. Zhao, J. Wang, Phys. Lett. A **323**, 285 (2004)
17. H.K. Zhao, Eur. Phys. J. B **33**, 365 (2003)
18. H.K. Zhao, J. Wang, Eur. Phys. J. B **9**, 513 (1999); H.K. Zhao, J. Wang, Phys. Rev. B **64**, 094505 (2001)
19. R. Saito, G. Dresselhaus, M.S. Dresselhaus, *Physical Properties of Carbon Nanotubes* (Imperial College Press, London, 1998)
20. X. Blase, L.X. Benedict, E.L. Shirley, S.G. Louie, Phys. Rev. Lett. **72**, 1878 (1994); Yu.A. Krotov, D.H. Lee, S.G. Louie, Phys. Rev. Lett. **78**, 4245 (1997)
21. M. Buongiorno Nardelli, Phys. Rev. B **60**, 7828 (1999); D. Orlikowski et al., Phys. Rev. B **63**, 155412 (2001)
22. J. Taylor, H. Guo, J. Wang, Phys. Rev. B **63**, 245407 (2001)
23. R. Egger, A.O. Gogolin, Phys. Rev. Lett. **79**, 5082 (1997); R. Egger, Phys. Rev. Lett. **83**, 5547 (1999)
24. C.L. Kane, L. Balents, M.P.A. Fisher, Phys. Rev. Lett. **79**, 5086 (1997)
25. M. Bockrath, D.H. Cobden, J. Lu, A.G. Rinzler, R.E. Smalley, L. Balents, P.L. McEuen, Nature (London) **397**, 598 (1999)
26. T.W. Odom, J.L. Huang, P. Kim, C.M. Lieber, J. Phys. Chem. B **104**, 2794 (2000)
27. A.-P. Jauho, N.S. Wingreen, Y. Meir, Phys. Rev. B **50**, 5528 (1994)
28. H.K. Zhao, Z. Phys. B **102**, 415 (1997); H.K. Zhao, Phys. Lett. A **226**, 105 (1997)
29. Q.F. Sun, J. Wang, T.H. Lin, Phys. Rev. B **59**, 3831 (1999)
30. R. Landauer IBM J. Res. Dev. **1**, 223 (1957); M. Büttiker, Phys. Rev. Lett. **57**, 1761 (1986)
31. J.P. Lu, Phys. Rev. Lett. **74**, 1123 (1995)
32. S. Roche, G. Dresselhaus, M.S. Dresselhaus, R. Saito, Phys. Rev. B **62**, 16092 (2000)